Tunnelling and Underground Space Technology 129 (2022) 104689

Contents lists available at ScienceDirect

Tunnelling and Underground Space Technology incorporating Trenchless Technology Research

journal homepage: www.elsevier.com/locate/tust

GPR surveys in enclosed underground sewer pipe space

Hengameh Noshahri *, Mark van der Meijde, Léon olde Scholtenhuis

University of Twente, Drienerlolaan 5, Enschede 7522 NB, the Netherlands

ARTICLE INFO

Keywords:
Ground Penetrating Radar
Subsurface void
In-pipe inspection systems
Concrete sewer pipes
gprMax

ABSTRACT

To identify voids around underground concrete sewer pipes, a few studies have introduced conducting in-pipe Ground Penetrating Radar (GPR) inspection systems along the pipes. However, less research has focused on studying the implications of emission, propagation, and reception of electromagnetic waves in the enclosed environment of sewer pipes and their subsequent impact on the resulting radargrams. We defined simulation scenarios where we examine the influence of longitudinal and rotational survey types, antenna frequency, air–gap between antenna and sewer wall, antenna separation, and pipe wall's mirroring effect on the resulting radargrams. Our results encourage practical considerations for designing in-pipe GPR surveys and outline the subsequent steps for automating the in-pipe GPR surveys.

1. Introduction

Sewer systems are one of the essential underground infrastructures in urban areas. Preserving the functionality of these systems requires regular inspection and maintenance of the pipelines and their surrounding ground (Noshahri et al., 2021). Sewer pipes are exposed to various loads during their life-cycle. Once these loads exceed the load carrying capacity of the pipe, failure mechanisms start which may lead to defects such as cracks in the fabric of the pipe (Tinga, 2013). Some of these cracks can form deep across the pipe wall and cause infiltration or exfiltration, depending on the water table level in the surrounding ground. The resulting water or sewage flow washes the soil around the sewer pipe and forms small voids.

Formation of underground voids around sewer pipes can lead to loss of structural integrity of the pipe and its adjacent ground (Guo et al., 2013). Identifying underground voids in their early stages of development can prevent these issues regarding pipe's structural integrity and their progressing into sinkholes. Assessing the environmental condition of sewer pipes is, therefore, an important factor in the holistic structural health monitoring of these assets (Davies et al., 2001; Noshahri et al., 2021). This assessment focuses on mapping the composition of ground layers and objects embedded within those layers.

Composition of the ground layers and objects, including the presence of leakages and voids, can be evaluated by running Ground Penetrating Radar (GPR) surveys (Lai et al., 2017). GPR is an electromagnetic (EM) inspection method that can help locate and assess conditions of underground assets, including sewer pipes (Liu and Kleiner, 2013).

In the GPR method a transmitter antenna (Tx) emits discrete pulses of energy in form of EM waves. Whenever there is a contrast between the dielectric properties of the mediums in which the wave is propagating, a part of the waves reflects and it is received by a receiver antenna (Rx). The receiver antenna of a GPR unit records the reflected EM waves in discrete sample points called traces. The distance the wave signal travels from the transmitter to an object to the receiver is called the reflection path, and the time it takes for the wave to travel the reflection path is called the Two-Way-Travel-Time (TWTT). Altogether, the results of GPR surveys can be displayed as a single trace at a specific location (called A-scan) or as a 2D plot of the TWTT of the EM waves across the traces along the GPR unit's path (called B-scan or radargram) (Reynolds, 2011).

The most common mode of operating a GPR unit is to tow it over the ground surface. Luo and Lai (2020);Jin-sung et al. (2020);Liu et al. (2021);Thitimakorn et al. (2016), for example, report successful detection of voids under the road using ground surface GPR surveys. However, while this method can locate shallow subsurface voids and deeper significant anomalies such as large voids and leakages, they are not suitable for identifying small voids and defects in the close vicinity of, and especially under, a sewer pipe which is buried 1–4 meters deep in the ground. This is because there is an inverse relation between the frequency of EM waves and the survey depth (Daniels, 2005). Low-frequency EM waves can propagate deeper into the ground, but due to their long wavelength they are less sensitive to small-scale structures, and the resulted radargrams will have a low resolution. Surveys with

* Corresponding author.
E-mail addresses: h.noshahri@utwente.nl (H. Noshahri), m.vandermeijde@utwente.nl (M. van der Meijde), l.l.oldescholtenhuis@utwente.nl (L. olde Scholtenhuis).

https://doi.org/10.1016/j.tust.2022.104689
Received 2 November 2021; Received in revised form 9 August 2022; Accepted 11 August 2022
Available online 23 August 2022

high-frequency EM waves, on the other hand, are limited in depth but can provide high-resolution results.

To better identify compositions of soil around the sewer pipes, and thus to identify early stages of formation of sinkholes, GPR surveys with high-frequency antennas can be done from inside the pipes (hereby called in-pipe GPR surveys). Studies such as (Koo and Ariaratnam, 2006), and (Jaganathan et al., 2010) have introduced in-pipe sewer GPR inspection systems. In this mode of operation, an antenna unit is carried inside and along the pipe by a human operator (for big pipe sizes) or by a crawler to scan the pipeline in a certain angular position. Even though a few studies report successful condition assessment and mapping of the pipe surroundings using this method (Ariaratnam and Guercio, 2006; Ékes et al., 2011; Ékes, 2016; Ékes, 2017), the consequences of conducting GPR surveys inside the enclosed space of the sewer pipe has received less attention to date.

Running in-pipe GPR surveys demands different measures compared to the ground surface surveys with respect to selecting survey's target depth and resolution, choosing antenna frequency, setting antenna configuration and antenna separation and setting up the survey path. These elements together with the physical behavior of the EM waves results in different reflection shapes and artifacts in the radargrams. This, in turn, demands taking different steps in signal processing and interpretation of the radargrams. Such steps have been developed in the literature only for more conventional ground-surface GPR surveys (Lai et al., 2018). Due to the different geometry for full 3D acquisition within a pipe we aim with this study to investigate the influences of an in-pipe operation environment on GPR survey design and subsequent analyses of the radargrams.

In the next section, we explain our methodology. Specifically, we describe the geometry and parameters used for testing different scenarios by means of numerical modeling. In Section 3, we show the results for each scenario and discuss what they imply for conducting in-pipe GPR surveys. Finally, we present the conclusions of this study and how it outlines the steps for future work.

2. Methods

2.1. Numerical modeling

We use numerical modeling in gprMax, which is an open source software that simulates EM wave propagation by solving Maxwell's equations using the Finite-Difference Time-Domain (FDTD) method (Warren et al., 2016). This facilitates a controlled and versatile environment where we can define various scenarios.

Each scenario is described by a geometry, survey variables, and a survey path. All geometries have a concrete pipe with inner diameter of 300[mm] and wall thickness of 31[mm] (a typical size for non-reinforced concrete pipe Holcim Australia, 2015) that is surrounded by dry sand with one or more spherical air pockets (with a radius of 20 [mm]). Further, survey variables consist of antenna frequency, size of the air–gap between the antenna and concrete wall, and the distance between the Tx and Rx antennas. For the survey path, in addition to the conventional longitudinal motion of the GPR unit, we introduce and study the rotational in-pipe survey path. In this type of survey path the GPR unit can be moved along the inner circumference of the pipe at any given location along the pipe. The advantage of this survey type is providing a 360 degree scan around the pipe.

To describe the geometry of the in-pipe GPR survey and to localize the voids, we use a cylindrical coordinate system as shown in Fig. 1. The position of every point, P, is described by three parameters: *radial position*, ρ, which is the distance between the projection of P on the xy-plane, P', and the origin (center of the sewer pipe), *angular position*, θ, which is the angle between x-axis and a line from the origin to P', and *axial position*, z, which is the height of the point on the pipe's axis, i.e., the distance between point P and the xy-plane.

For studying the longitudinal and rotational 2D scenarios we use the same geometry as the 3D case (Fig. 1) but reduced to yz- and xy- planes. The baseline modeling parameters and survey variables are given in Table 1. Table 2 gives an overview of the studied scenarios and explains how they deviate from the baseline. Table 3 presents the schematic drawings of the modelled scenarios.

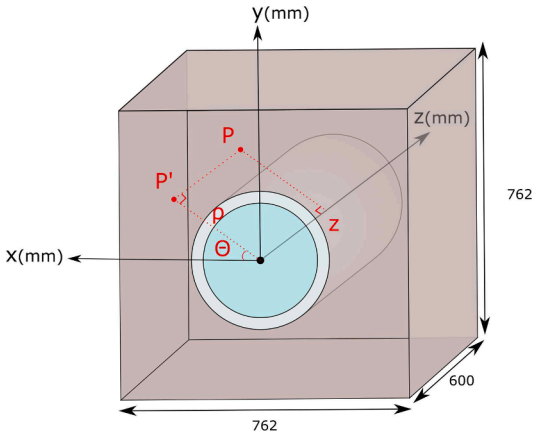

Fig. 1. Baseline geometry, Air: blue, Concrete: gray, Soil: brown. Any point P is described by (ρ, θ, z) in the cylindrical coordinate system.

2.2. Signal processing

Detection of objects in the radargrams is done by examining the polarity of the reflections. The reflected wave has an amplitude and polarity according to Eq. 1.

$$R = \frac{\sqrt{\epsilon_2} - \sqrt{\epsilon_1}}{\sqrt{\epsilon_2} + \sqrt{\epsilon_1}} \tag{1}$$

where R (reflection coefficient) is the proportion of energy reflected, ϵ_1 and ϵ_2 are the respective relative dielectric constants of the host and target, respectively (Reynolds, 2011). Detecting a change in the amplitude and polarity of the incident wave using this equation is the key to interpreting GPR survey results.

To illustrate this better, we consider an example with a geometry similar to scenario 2 in Table 3. We run a 2D longitudinal survey using the baseline parameters as given in Table 1. Fig. 2a shows the raw electromagnetic field values alongside the A-scan at trace 145 (where

Table 1
Baseline model parameters and survey variables

	2D		3D	
	longitudinal	rotational	longitudinal	rotational
Domain size	$600[mm] \times 762[mm]$	$762[mm] \times 762[mm]$	$600[mm] \times 762[mm] \times 762[mm]$	
Yee cell size	$1[mm] \times 1[mm]$		$2[mm] \times 2[mm] \times 2[mm]$	
Number of traces	289	360	289	360
Survey path	$\rho = 150, \theta = 3\pi/2$	$\rho = 150, z = 0$	$\rho = 150, \theta = 3\pi/2$	$\rho = 150\ z = 100, 200, 300, 500$
start(first trace)	$z = 0$	$\theta = 0[deg]$	$z = 0$	$\theta = 0[deg]$
end(last trace)	$z = 600$	$\theta = 360[deg]$	$z = 600$	$\theta = 360[deg]$
Waveform	Ricker			
Antenna frequency	$2[GHz]$			
Antenna separation	$0[mm]$			
Air–gap	$0[mm]$			
Shielded antenna?	No			

Table 2
The first column indicates if the survey path is longitudinal or rotational. The second column indicates if the model is 2D or 3D. The third column indicates the aim of studying this scenario (e.g., to investigate the effect of changing a survey variable) and the next column gives additional information about the modified values in the scenario. The fifth column provides information about the air voids around the pipeline by defining the position of the center of spherical voids $(\rho[mm], \theta[rad], z[mm])$.

Survey path type	Simulation type	Subject of study	Variable values	Void(s) location	Scenario number
Longitudinal	2D	Antenna frequency	$0.5, 1, 2[GHz]$	$(231, 3\pi/2, 144)$ $(281, 3\pi/2, 300)$ $(331, 3\pi/2, 444)$	1
		Air–gap	$2[GHz]$ $0, 100[mm]$	$(281, 3\pi/2, 300)$	2
			$1[GHz]$		3
		Antenna separation	$0, 100[mm]$	$(281, 3\pi/2, 300)$	4
		Pipe wall's mirroring effect		$(231, 3\pi/2, 144)$ $(331, \pi/2, 444)$	5
	3D	General comparison with 2D		$(231, 3\pi/2, 144)$ $(281, 3\pi/2, 300)$ $(331, 3\pi/2, 444)$	6
Rotational	2D	Air–gap	$0, 100[mm]$	$(281, \pi, 300)$	7
		Antenna separation	$0, 100[mm]$	$(281, \pi, 300)$	8
		Pipe wall's mirroring effect		$(281, 3\pi/2, 300)$	9
	3D	Distance between object plane and survey path	$0, 100, 200, 400[mm]$	$(281, \pi, 100)$	10

Table 3
Schematic drawings of the scenarios - Air: blue, Concrete: gray, Soil: brown

Longitudinal

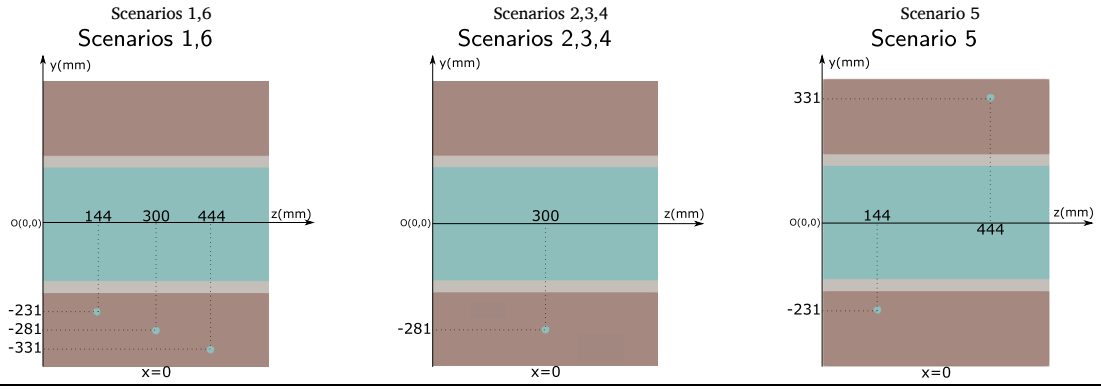

Rotational

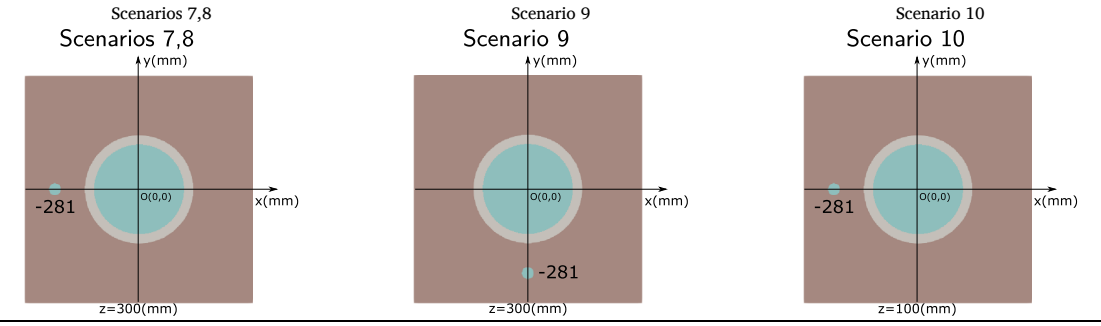

the center of the air void is). It can be seen that the contrast between the reflection from the air void is not clearly visible. To enhance the signal we multiply the field values with a gain that compensates for exponential attenuation of the signal amplitude with increasing TWTT. We also apply filtering in frequency domain to remove the horizontal lines that appear in the radargram due to reverberation from the concrete pipe (Noshahri et al., 2020) (such region with reverberation lines is shown with an arrow in Fig. 2a). The result of these two processing steps is shown in Fig. 2b.

The arrival time of the hyperbolic reflection due to the air void is also shown both in the radargram and A-scan of Fig. 2b. It can be seen that the polarity of the signal changes at this time because $\epsilon_{sand} = 3$ and $\epsilon_{air} = 1$ and therefore $R < 0$ in Eq. 1.

In the remainder of this paper, only the processed radargram will be displayed.

2.3. Visualizing rotational radargrams

The radargrams of longitudinal surveys are made by plotting the TWTT of the EM waves across the traces along the GPR unit's path. This is the conventional *rectangular* radargram representation (as seen in the example radargram of Fig. 2), where the trace numbers have a linear relation with the distance travelled by the GPR unit.

Unlike the longitudinal surveys, visualizing the results of rotational surveys is not straightforward. One approach is to use a *circular cross-sectional* plot to represent the circular geometry of the pipe's cross-section. In this case, traces are mapped to the angular position, and TWTTs are mapped to the radial position in a polar coordinate system. Fig. 3a uses this approach to visualize the rotational survey result for an example with a geometry similar to scenario 7 in Table 3. In this scenario, a void is located at $180[deg]$. The advantage of this representation

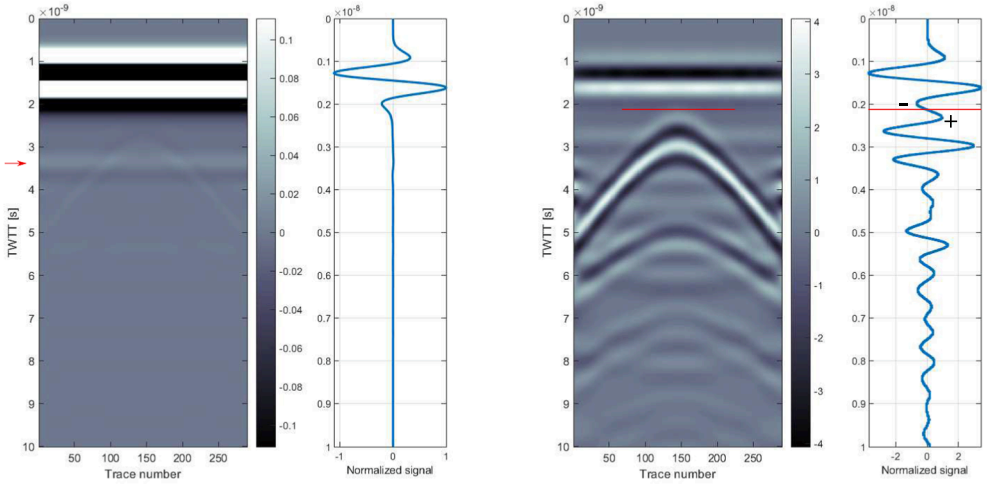

(a) Left: Raw radargram, Right: Trace 145 (b) Left: Processed radargram, Right: Trace 145

Fig. 2. Signal processing steps on an example radargram.

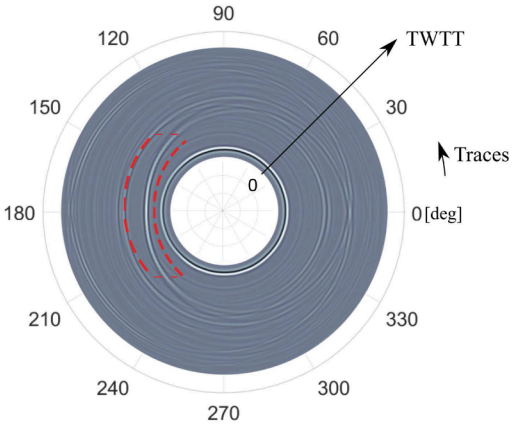

(a) Circular cross-sectional plot

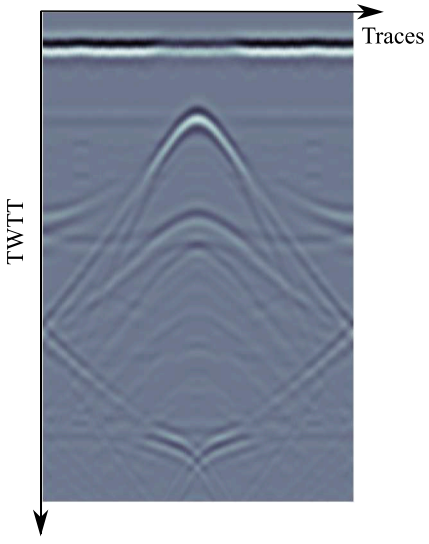

(b) Rectangular plot

Fig. 3. Two types of representation for rotational survey radargram.

is that it reveals the position of the void in relation to the pipe and the actual geometry of the pipe's cross section. However, the reflection from the void (marked between the dashed lines in Fig. 3a) is no longer seen as a hyperbola, because it is distorted and stretched. Therefore, the presence of the void is not easily discernible when a *circular cross-sectional* representation is used.

Another approach for visualizing the results of rotational surveys is to use the *rectangular* plot similar to the longitudinal survey radargrams. Fig. 3b visualizes such plot for the example with a geometry similar to scenario 7 in Table 3. This representation no longer gives a direct insight about the geometry of the pipe and the location of the void. Besides, the trace number in the horizontal axis is a function of the pipe diameter and it has a non-linear relation to the actual travel distance of the GPR unit. However, the hyperbolic reflection from the void is not distorted and can clearly be seen, and hence, the survey result is easier to interpret.

To highlight the effects of rotational survey paths, in the remainder of this work, we use the *rectangular* plot for rotational survey radargrams.

3. Results and discussion

This section presents the results from the simulated scenarios, organized by the subjects presented in column 3 of Table 2.

3.1. Longitudinal 2D

3.1.1. Antenna frequency (scenario 1)

In this scenario, three voids are present in the sand below the sewer pipe at radial distances of $50, 100$, and $150[mm]$ from the pipe wall (see Table 2 and 3). Fig. 4a, 4b, and 4c show the radargrams of running longitudinal survey with antenna frequency of $500[MHz], 1[GHz]$, and $2[GHz]$, respectively. In Fig. 4a the reflections of three voids cannot be discerned individually. In contrast, using antenna frequency of $2[GHz]$, as shown in Fig. 4c, increases the resolution and causes each hyperbolic reflection to be easily distinguished from the background and from the other reflections.

In general, antenna frequency should be chosen according to the depth and minimum size of the void that has to be detected and by calculating the radar's footprint (Luo et al., 2020). Fig. 5 shows minimum detectable void size for voids that are $50, 100$ and $150[mm]$ away from the pipe wall for a range of antenna frequencies and has been made based on the method proposed by Luo et al. (2020). It is also apparent from this figure that a $2[GHz]$ survey is suitable for the void size (with a

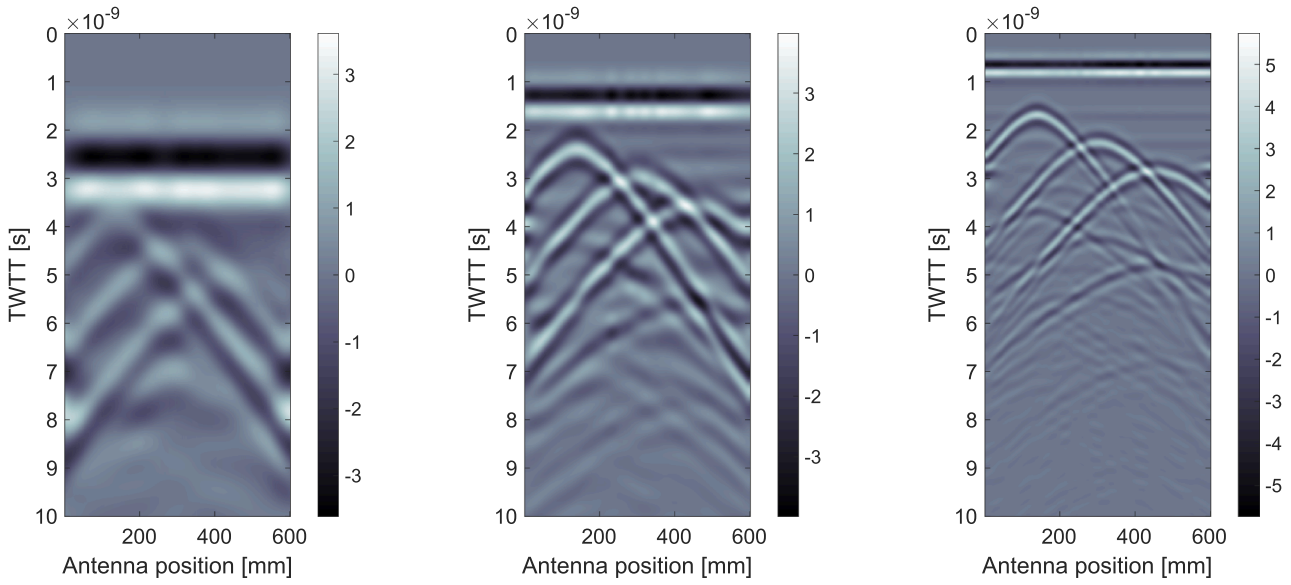

(a) 500[MHz] (b) 1[GHz] (c) 2[GHz]

Fig. 4. Results of scenario 1, the effect of antenna frequency on the hyperbolic reflections of three voids at different radial distances - longitudinal 2D survey.

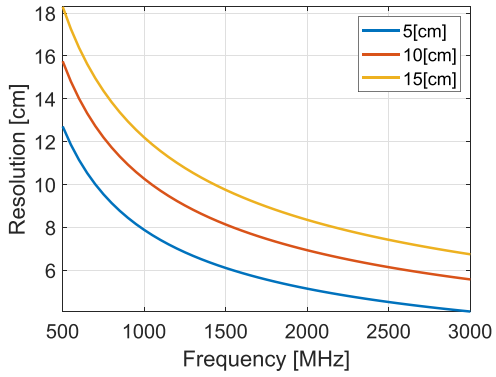

Fig. 5. Minimum detectable void sizes vs. antenna frequency for various radial distances.

diameter of 40[mm]) and depths (50 −150[mm]) that are defined in our scenarios.

3.1.2. Air–gap (scenario 2 and 3)

Unlike a ground surface survey, it might not be possible to have the GPR transmitter and receiver flat to the surface inside the sewer pipe. Due to the rounded walls of the pipe there will probably be an air–gap between the transmitter–receiver and the pipe wall. We study the effect of having an air–gap in a 2D longitudinal survey for two different antenna frequencies. To keep the geometry simple we only model one air void in the substrate (see Table 2 and 3). Fig. 6 shows the results with 0 and 100[mm] air–gap and an antenna frequency of 2[GHz] (scenario 2). We observe that increasing the air–gap (from Fig. 6a to Fig. 6b) distorts the shape of reflection. It becomes flatter or stretched horizontally, thereby reducing the detection capability and accurate location estimate. Reducing the antenna frequency to 1[GHz] (scenario 3) and increasing the air–gap (from Fig. 7a to Fig. 7b) makes the reflection coarser and further deteriorates the reflection shape's integrity.

The results indicate that during a survey the GPR antennas should be kept in contact with the pipe wall. If having an air–gap is inevitable it is advisable to use higher frequency antennas, which are also smaller and hence can be placed closer to the pipe wall, and thereby can limit the adverse effects of air–gap on the radargrams.

3.1.3. Antenna separation (scenario 4)

For practical purposes the transmitter and receiver can be combined in one single antenna or they can be separate from each other. We have modelled the possible effect of 100[mm] antenna separation versus a combined Tx-Rx antenna over a single air void (Fig. 8).

It can be observed that due to the longer path that EM waves have to travel to reach from the Tx to the Rx antenna, the hyperbolic shape of reflection looks a bit stretched. The longer path also makes the waves to arrive with a bit of delay compared to when the antenna separation is zero.

The shape of the parabola, next to the flattening, does not change and no artefacts are created. This can be clearly seen in the similarity between the reflection shapes in Fig. 8b and Fig. 8a, contrary to the distortions as observed when an air–gap is present (Fig. 6b and 7b).

Therefore, if a trade-off has to be made in the survey design between air–gap and antenna separation, it is better to eliminate the air–gap and keep the antennas separated.

3.1.4. Pipe wall's mirroring effect (scenario 5)

In all previous cases, the geometry only included air voids which were located on one side of the sewer pipe – specifically, bellow it. In this scenario we investigate a phenomenon that is unique to the in-pipe GPR survey with unshielded antenna with one void below the pipe and another void at the opposite side, on top of the pipe (see Table 2 and 3).

Fig. 9 shows the resulting radargram. The hyperbola visible on the left half of the radargram (with its apex at the location of 145[mm]) is similar to what we have modelled before and it is related to the air void bellow the pipe. The reflection of the air void at top of the pipe (located in between the dashed lines in Fig. 9) arrives later in time. This reflection is also wider and less steep, which can be geometrically explained by the fact that the second air void is further away from the antenna and the reflection path length varies less when moving the antenna horizontally.

While the information about the axial position of voids can be retrieved from the results of a longitudinal survey, conducting this survey is by no means sufficient to know the angular - and hence, the full 3D - location of the voids. The hyperbola in the right side of Fig. 9 (with its apex at the location of 445[mm]) could have been as well related to a deeper and bigger void below or on one of the sides of the pipe.

Using a shielded antenna can solve the problem of uncertainty about the 3D position of the void. However, to scan the entire area around the

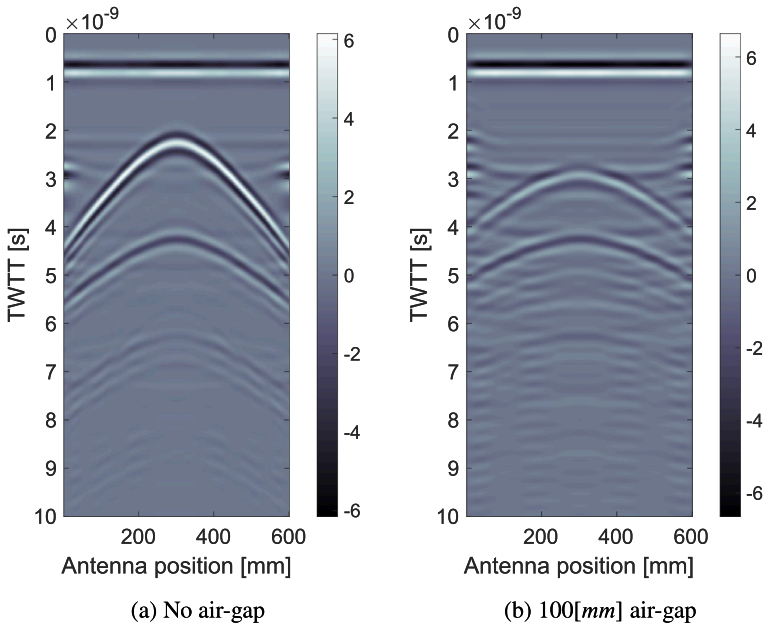

Fig. 6. Results of scenario 2, the effect of air–gap and a survey frequency of 2[*GHz*] on the hyperbolic reflection of a single void - longitudinal 2D survey.

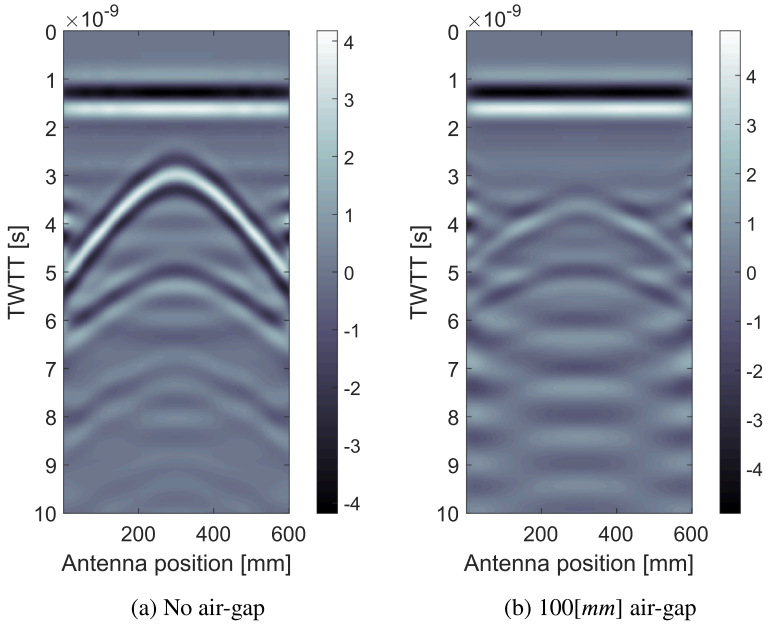

Fig. 7. Results of scenario 3, the effect of air–gap and a survey frequency of 1[*GHz*] on the hyperbolic reflection of a single void - longitudinal 2D survey.

sewer pipe, the longitudinal survey must be repeated for multiple angles inside the pipe.

3.2. Longitudinal 3D (scenario 6)

This scenario is identical to the case of longitudinal 2D survey with three voids in the substrate with the difference of one additional spatial dimension (see details in Table 2). It can be seen in Fig. 10 that there is more noise in 3D compared to 2D. This is because the energy that gets transmitted in the 2D simulation dissipates in the absorbing boundaries of the model and does not get back to the receiver. But in the simulated 3D case, where this absorbing boundary is not present, the waves get reflected from the sewer wall and cause interference. Using a shielded antenna can partly alleviate these artefacts.

3.3. Rotational 2D

3.3.1. Air–gap (scenario 7)

In this scenario we investigate the effect of having an air gap between the antenna and the sewer pipe when conducting a rotational survey. The results of 2D numerical modeling for a rotational survey with 2[*GHz*] antenna frequency and 0 and 100[*mm*] gap between the antenna and pipe wall can be seen in Fig. 11a and 11b, respectively.

Same as scenario 2 with the longitudinal survey, we observe that the presence of an air–gap distorts the shape of the reflection. Comparing Fig. 11b to Fig. 6b reveals that air–gap adversely affects the 2D rotational radargram more than its longitudinal counterpart. This is because the reflections paths are intrinsically longer in the rotational case due to the curvature of the sewer wall (Noshahri et al., 2020). Hence, it is important to try to keep the air–gap zero in rotational in-pipe GPR

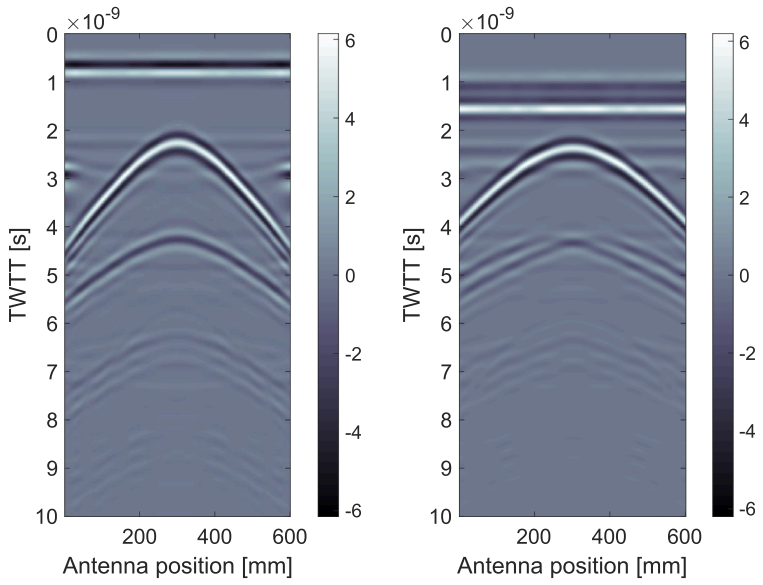

(a) Single antenna (b) 100[*mm*] antenna separation

Fig. 8. Results of scenario 4, the effect of antenna separation on the hyperbolic reflection of a single void - longitudinal 2D survey.

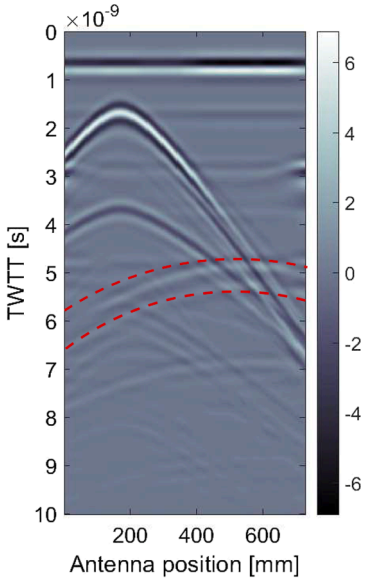

Fig. 9. Result of scenario 5, pipe wall's mirroring effect with one void below and one void on top of the sewer pipe - longitudinal 2D survey.

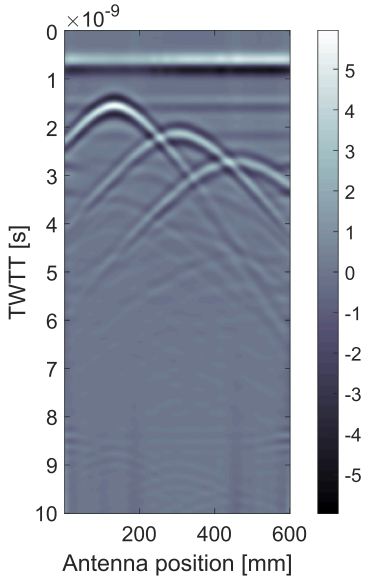

Fig. 10. Result of scenario 6, the effect of running a simulation in 3D - longitudinal survey.

surveys.

3.3.2. *Antenna separation (scenario 8)*

In this scenario of a rotational 2D survey, we study the possible effect of an antenna separation of 100[*mm*] versus when the Tx and Rx are together. Similar to the longitudinal case (scenario 4, see Fig. 8), it can be observed in Fig. 12 that the distance between the antennas does not influence the reflection shapes of the air voids - the integrity of the hyperbolic shape is intact and not distorted.

Therefore, similar to the longitudinal survey, if a trade-off has to be made in a rotational survey in the design of GPR antennas between air–gap and antenna separation, it is better to keep the air–gap as small as possible and add antenna separation.

3.3.3. *Pipe wall's mirroring effect (scenario 9)*

In this scenario we investigate how the pipe wall acts like a mirror and how the reflections from voids across the pipe appear in the resulting radargrams when doing rotational in-pipe surveys with unshielded antennas.

The geometry of this scenario consists of a void at the bottom of the sewer pipe (see Table 2 and 3). Therefore, we expect to see a hyperbolic reflection with its apex at 270[*deg*] which is apparent in Fig. 13. Besides this reflection, we also see an inverted hyperbola with an apex at 90[*deg*] which is the same air void but seen from 180[*deg*] away from the voids rotational location.

When we compare this result with scenario 5, where longitudinal survey was conducted, we can see that unlike a longitudinal survey, a rotational survey can provide information about the angular position of the void.

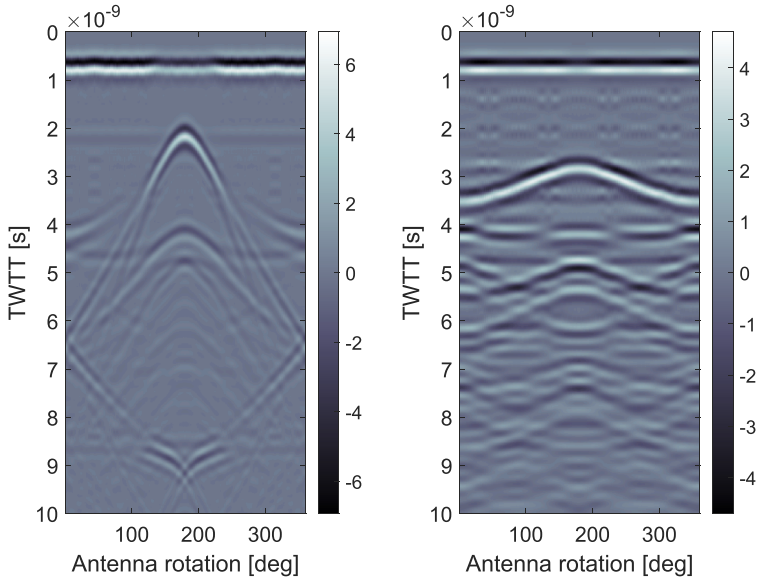

(a) No air-gap (b) 100[mm] air-gap

Fig. 11. Results of scenario 7, the effect of air–gap on the hyperbolic reflection of a single void - rotational 2D survey.

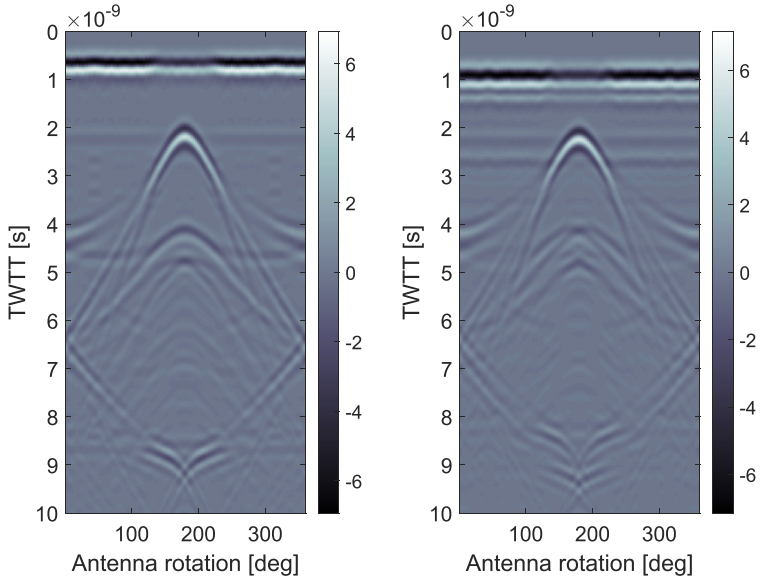

(a) Single antenna (b) 100[mm] antenna separation

Fig. 12. Results of scenario 8, the effect of antenna separation on the hyperbolic reflection of a single void - rotational 2D survey.

3.4. Rotational 3D (scenario 10)

The knowledge gained from studying the topics of antenna frequency, antenna separation, and air–gap can be extended to the 3D rotational surveys as well. For this case, we only study the effect of the longitudinal distance between the void and the survey path. Unlike the 2D scenarios where the void and the survey path were both in one plane, in the 3D rotational case there can be an axial distance between the plane where the object is located and the plane where the survey path is defined.

Fig. 14 illustrates this point and describes the geometry. In this scenario, a spherical void is placed at $(\rho, \theta, z) = (281, \pi, 100)$ (see Table 2). We test four surveys. In all cases, the antenna is rotated in a plane parallel to xy-plane. The first survey path - or Antenna Plane (AP)- is at $z = 100[mm]$, so at the same axial position as the void (i.e., the same plane as the Object Plane (OP)). AP2, AP3, and AP4 are located at 100, 200, and 400[mm] away, respectively.

The results of these four surveys are shown in Fig. 15. The reflection from the void can be seen in all figures at 180[deg] but the time when the reflection arrives, and also the width of the hyperbola increase from Fig. 15a to Fig. 15d. This happens because increasing the distance between the antenna and the void naturally increases the reflection path and makes the reflection shape more flat.

It can be concluded that, while conducting a rotational survey can specify the angular position of the void, a single rotational survey is not sufficient for knowing the axial position of it. The reflection seen in Fig. 15d could have as well been related to a deeper void at $z = 500[mm]$. Hence, to get full (3D) information about the void's location, the rotation of the antenna must be repeated at various axial positions along the pipe. The exact axial position of a void can then be determined

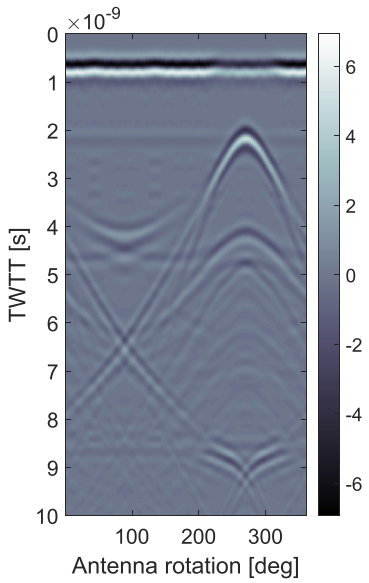

Fig. 13. Result of scenario 9, pipe wall's mirroring effect with one void below the sewer pipe - rotational 2D survey.

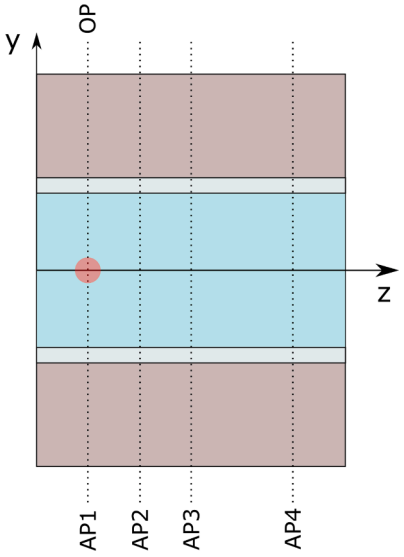

Fig. 14. Geometry of scenario 10 (side view), Object Plane (OP) is at $z = 100[mm]$, Antenna Plane (AP)1–4 are $0, 100, 200$, and $400[mm]$ away from the OP, respectively.

by knowing the axial position of the survey path which results in the shallowest reflection.

4. Conclusions

In this study, we looked at the implications of running GPR surveys from inside the sewer pipes for the purpose of identifying early stages of air void formation around the pipes. Previous studies similarly have focused on void identification in the subsurface environment using GPR surveys. However, their method is mostly suitable for shallow voids directly under the road rather than deeper voids which can form around the pipes.

To contribute to the literature on void detection, this study (1) quantifies parameters of antenna frequency, air gap, antenna separation, pipe wall's mirroring effect for in-pipe survey design, (2) introduces in-pipe rotational survey, which involves moving the GPR unit along the inner circumference of the pipe at any given location along the pipe, and (3) gives insights on how a void behind a sewer pipe appears in an in-pipe GPR survey.

We defined ten simulation scenarios where we examine the influence of survey type, antenna frequency, air–gap between antenna and sewer wall, antenna separation, and pipe wall's mirroring effect on the resulting radargrams. Our results lead to practical suggestions prior to conducting in-pipe GPR surveys inside the sewer pipe.

First, the results show that the radargram resolution provided by an antenna with at least a frequency of $2[GHz]$ is required for distinguishing the air voids which are at close proximity of the sewer wall or directly behind it. In general, antenna frequency should be selected based on the minimum size of the voids that need to be detected and their radial distance from the sewer pipe (as shown in the example of Fig. 5).

Second, given the curved geometry of the sewer pipe, it might not be possible to keep the GPR unit in contact with the pipe wall during the surveys. Having an air–gap distorts the shape of the hyperbolic reflections and adds additional artifacts to the radargram which can adversely affect identifying the air void and its location and size. Due to naturally longer reflection path, this influence is considerably more when conducting a rotational survey.

Third, separating the transmitter and receiver antenna shifts down the apex of the hyperbola (i.e., the reflection arrives later in time) and stretches it horizontally. However, this does not have a substantial effect in identification of the air void as much as adding an air–gap. Therefore, if a trade-off has to be made in the survey design between antenna separation and air–gap, it is better to try to reduce the air–gap as much as possible.

Another phenomenon which is unique to in-pipe GPR surveys with unshielded antennas is the sewer wall's mirroring effect. For a longitudinal survey, the hyperbolic reflections which appear in the radargrams can equally be attributed to an air void under the antenna or an air void on the other side of the sewer pipe. Therefore, a longitudinal survey can specify the axial position of the voids but it cannot specify their angular position. To achieve information about the 3D location of the air voids from a longitudinal survey, the survey has to be repeated for different angles.

Rotational survey, however, can specify the angular position of the voids. This is because when the GPR antennas are $180[deg]$ away from an air void, the reflection from the void appears as an inverted hyperbola. The time of arrival of the apex of the void's hyperbolic reflection is shortest at its angular position. The shortcoming of the rotational survey is its inability in determining the axial position of the air voids. This means that a hyperbolic reflection at a certain angular position can be attributed to an air void which is axially away from the antenna plane or an air void which is at a larger radial position. Therefore, to achieve information about the full 3D location of the air voids from a rotational survey, the survey has to be repeated for different axial positions along the pipe.

Table 4 summarizes the findings of this paper on each topic and has technical implications for in-pipe GPR survey design.

Future work should run experimental surveys in order to verify these effects in practice. To do so, an automatic solution should be developed that can traverse inside the sewer pipes and run both longitudinal and rotational surveys remotely. Since rotational and longitudinal surveys each provide part of the location information, combining both motions and running a helical survey will provide complete 3D information about the location of the voids. Running such survey can also be more efficient in terms of the survey time and, hence, important from a practical point of view. The possibility of this survey will be investigated as a future work.

Throughout this paper, we presented the radargrams of rotational surveys with rectangular plots. This enabled us to perform a more holistic comparison between the results of rotational and longitudinal surveys. The rectangular representation of rotational surveys also makes it easier to identify the hyperbolic reflection of the voids. However,

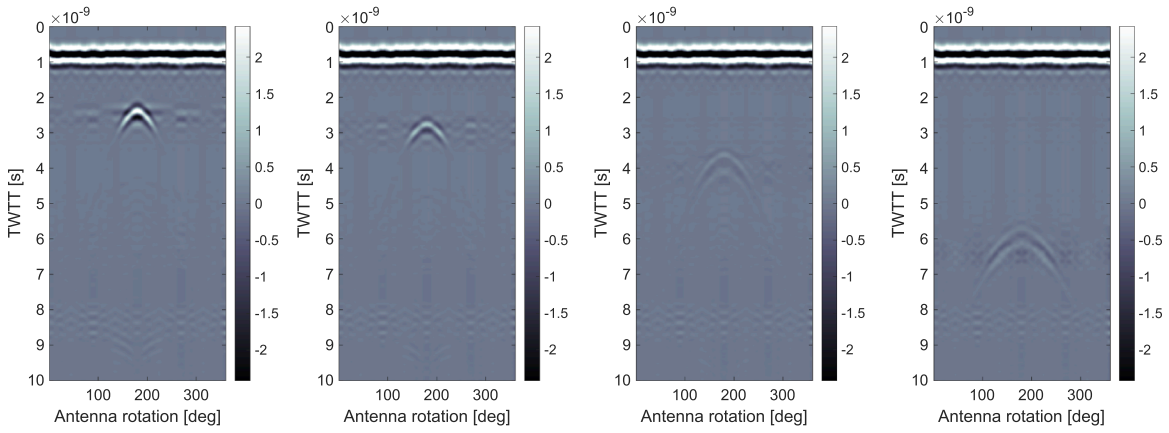

Fig. 15. Results of scenario 10, the effect of axial distance between the object plane and survey path - rotational 3D survey.

Table 4
Summary of the results

Survey variable	Findings
Antenna Frequency	Should be chosen based on size and radial distance of the target voids. For voids directly behind the sewer wall higher frequencies provide better resolution.
Air–gap	Distorts hyperbolic reflections and must be kept at minimum (preferably zero).
Antenna separation	Does not distort the hyperbolic reflections. Can be non-zero.
Survey path	Longitudinal surveys can determine axial location of voids. Rotational surveys can determine angular position of voids.

circular cross-sectional representation has added benefits for a full 3D visualization of the survey results, because it connects the GPR data to the actual geometry of the pipe and its surrounding environment. Therefore, for visualization and asset management purposes, it might be worthwhile exploring in future work whether professionals in the field favour rectangular or circular cross-sectional plots.

Finally, although this paper provides a novel approach to void detection around sewer pipes, we acknowledge that other techniques could complement the GPR-based void detection as well. There is potential to enrich the literature by exploring new techniques and methodologies – such as acoustic profiling – and assess how data gathered from these, complement the state-of-the-art methods.

Declaration of Competing Interest

The authors declare that they have no known competing financial interests or personal relationships that could have appeared to influence the work reported in this paper.

Acknowledgments

This work was conducted as part of the Cooperation Programme TISCA (Technology Innovation for Sewer Condition Assessment) with project number 15393, which is (partly) financed by NWO domain TTW (the domain Applied and Engineering Sciences of the Netherlands Organisation for Scientific Research), the RIONED Foundation, STOWA (Foundation for Applied Water Research) and the Knowledge Program Urban Drainage (KPUD).

References

Ariaratnam, S.T., Guercio, N., 2006. In-pipe ground penetrating radar for non-distructive evaluation of PVC lined concrete pipe. Advances in Engineering Structures, Mechanics & Construction 140, 763–772. https://doi.org/10.1007/1-4020-4891-2_64.

Daniels, D.J., 2005. Ground Penetrating Radar. The Institution of Electrical Engineers, London, UK. https://doi.org/10.1002/0471654507.eme152. ISBN: 0 86341 360.

Davies, J.P., Clarke, B.A.,Whiter, J.T., Cunningham, R.J., 2001. Factors influencing the structural deterioration and collapse of rigid sewer pipes. Urban Water, 3 (1–2)(1–2): 73–89. ISSN 14620758. doi: 10.1016/s1462-0758(01)00017-6.

Ékes, C., Neducza, B., Henrich, G.R., 2011. GPR goes underground: pipe penetrating radar. In North American Society for Trenchless Technology (NASTT) No-Dig Show, Washington, D.C. https://sewervue.com/papers/B-3-02_Final_Paper_GPR_Goes_Underground-Pipe_Penetrating.pdf. (Accessed 14 July 2021).

C. Ékes. Sinkhole locating and corrosion quantification with pipe penetrating radar. In: Pipelines 2017: Condition Assessment, Surveying, and Geomatics, Proceedings of Sessions of the Pipelines Conference, pages 1–11, Phoenix, Arizona, USA, 2017. doi: 10.1061/9780784480885.001.

C. Ékes. Quantitative pipe condition assessment with pipe penetrating radar. In North American Society for Trenchless Technology (NASTT) No-Dig Show, Dallas, Texas, USA, 2016. URL https://sewervue.com/papers/Quantitative_pipe_condition_assessment_with_Pipe_Penetrating_Radar_No-Dig2016.pdf. (Accessed 14 July, 2021).

S. Guo, Y. Shao, T. Zhang, D.Z. Zhu, and Y. Zhang. Physical modeling on sand erosion around defective sewer pipes under the influence of groundwater. Journal of Hydraulic Engineering, 139 (12)(12):1247–1257, 2013. ISSN 0733–9429 1943–7900. doi: 10.1061/(asce)hy.1943-7900.0000785.

Holcim Australia. Concrete pipe reference manual. Brochure, 2015. https://www.holcim.com.au/sites/australia/files/atoms/files/hu-concrete-pipe-reference-manual-iss1.pdf. Accessed: 12-04-2022.

Jaganathan, A.P., Allouche, E., Simicevic, N., 2010. Numerical modeling and experimental evaluation of a time domain UWB technique for soil void detection. Tunn. Undergr. Space Technol. 25 (6(6)), 652–659. https://doi.org/10.1016/j.tust.2009.08.006. ISSN 08867798.

Jin-sung, Y., Minkyo, Y., Sehwan, P., Junkyeong, K., 2020. Technique for detecting subsurface cavities of urban road using multichannel ground-penetrating radar equipment. Sensors and Materials 32 (12). https://doi.org/10.18494/sam.2020.3081. ISSN 0914-4935.

Koo, D., Ariaratnam, S.T., 2006. Innovative method for assessment of underground sewer pipe condition. Automation in Construction 15 (44), 479–488. https://doi.org/10.1016/j.autcon.2005.06.007. ISSN 09265805.

Lai, W.W.L., Chang, R.K.W., Sham, J.F.C., 2017. Detection and imaging of city's underground void by GPR. In: 9th International Workshop on Advanced Ground Penetrating Radar (IWAGPR), pp. 1–6. https://doi.org/10.1109/IWAGPR.2017.7996055.

Lai, W.W.L., Dérobert, X., Annan, P., 2018. A review of ground penetrating radar application in civil engineering: A 30-year journey from locating and testing to imaging and diagnosis. NDT & E Int., 96:58–78. ISSN 09638695. doi: 10.1016/j.ndteint.2017.04.002.

Liu, Z., Kleiner, Y., 2013. State of the art review of inspection technologies for condition assessment of water pipes. Measurement 46 (1(1)), 1–15. https://doi.org/10.1016/j.measurement.2012.05.032. ISSN 0263–2241.

Liu, H., Shi, Z., Li, J., Liu, C., Meng, X., Du, Y., Chen, J., 2021. Detection of road cavities in urban cities by 3D ground-penetrating radar. Geophysics 86 (3), WA25–WA33. https://doi.org/10.1190/geo2020-0384.1. ISSN 0016–8033 1942–2156.

Luo, T.X.H., Lai, W.W.L., 2020. GPR pattern recognition of shallow subsurface air voids. Tunn. Undergr. Space Technol. 99 https://doi.org/10.1016/j.tust.2020.103355. ISSN 08867798.

T.X.H. Luo, W.W.L. Lai, and A. Giannopoulos. Forward modelling on gpr responses of subsurface air voids. Tunnelling and Underground Space Technology, 103, 2020. ISSN 08867798. doi: 10.1016/j.tust.2020.103521.

Noshahri, H., van Delft, M., Olde Scholtenhuis, L., Franco Hempenius, J., Dertien, E., 2020. Towards underground void detection with in-pipe ground penetrating radar.

In: In 3rd Asia Pacific Meeting on Near Surface Geoscience & Engineering, Thailand. https://doi.org/10.3997/2214-4609.202071025.

Noshahri, H., Olde Scholtenhuis, L., Doree, A., Dertien, E., 2021. Linking sewer condition assessment methods to asset managers' data-needs. Autom. Constr. 131 (103878) https://doi.org/10.1016/j.autcon.2021.103878.

J. Reynolds. An Introduction to Applied and Environmental Geophysics. John Wiley & Sons, Ltd., West Sussex, UK, 2nd edition, 2011. ISBN: 978-0-471-48535-3.

Thitimakorn, T., Kampananon, N., Jongjaiwanichkit, N., Kupongsak, S., 2016. Subsurface void detection under the road surface using ground penetrating radar (GPR), a case study in the Bangkok metropolitan area, Thailand. Int. J. Geo-Eng. 7 (1) https://doi.org/10.1186/s40703-016-0017-8. ISSN 2092–9196 2198–2783.

T Tinga. Principles of Loads and Failure Mechanisms; Applications in Maintenance, Reliability and Design. Springer Series in Reliability Engineering. Springer, London, UK, 2013. doi: 10.1007/978-1-4471-4917-0.

Warren, C., Giannopoulos, A., Giannakis, I., 2016. gprMax: Open source software to simulate electromagnetic wave propagation for ground penetrating radar. Comput. Phys. Commun. 209, 163–170. https://doi.org/10.1016/j.cpc.2016.08.020. ISSN 00104655.